Chapter 6

The contribution of coherent particle scattering to the reflections of radio waves by clouds

Abstract. *Well-known scattering mechanisms in clouds are Rayleigh scattering by individual droplets and clear-air scatter by spatial humidity variations. This chapter discusses the importance of these two mechanisms compared to a third scattering mechanism: coherent particle scattering by spatial variations in the liquid water content of the clouds. We will argue that for radars using a wavelength larger than a centimetre coherent particle scatter can dominate Rayleigh scattering from individual droplets, both for cumulus and stratiform clouds. Furthermore, this work will show that "clear-air" scatter is probably less important in clouds than previously thought. These conclusions are somewhat tentative, as there is an enormous lack of quantitative data on the spatial variations in humidity and liquid water content for the various cloud types. Especially simultaneous measurements of these spatial variations are needed.*

6.1 Introduction

Radars are much used in cloud research for the measurement of macroscopic and microscopic cloud properties, often in combination with other instruments like a lidar, or a radio wave radiometer. For most of these applications the scattering mechanism of the radio waves has to be understood well. Well-known mechanisms are incoherent particle scatter and coherent air scatter.

Incoherent particle scatter comes from particles (e.g. cloud droplets) which are randomly distributed within the radar volume. For small particles it is normally called

Rayleigh scatter, for larger ones Mie scatter. Incoherent particle scatter is most important for atmospheric radars with a small wavelength.

Coherent air scatter is caused by variations in the refractive index of atmospheric gases. This type of scatter is often called Clear-air scatter or Bragg scatter. In this thesis it will be called coherent air scatter. Coherent air scatter is normally dominated by spatial variations in humidity, but also variations in temperature and pressure can play a role, as well as the co-variances between these three variables [Gossard and Strauch, 1980]. Coherent air scatter occurs mainly in radar measurements using a long wavelength (cm-waves or longer).

Chapter 5 showed showed that a third scattering mechanism may be important in clouds: coherent particle scatter by variations in the liquid water content (LWC) of clouds. Just as coherent air scatter, this mechanism is mainly important for atmospheric radars with a long wavelength. Chapter 5 showed that coherent particle scatter (scatter of radio waves by spatial variations in particle mass density) can explain the dual-wavelength radar measurements of cumulus clouds performed by Knight and Miller (1998) and those of a smoke plume by Rogers and Brown (1997). Chapter 5 also showed quantitatively that for an S-band radar, coherent particle scatter can be stronger than incoherent particle scatter in a cumulus cloud. Moreover, it showed that coherent particle scatter can be stronger than coherent (clear-) air scatter at the top of a cumulus cloud.

We argue that together the measurements and theory offer a strong case that coherent particle scatter is significant in S-band radar measurements of cumulus clouds. That is why in this work we will explore the importance of this scattering mechanism for other radar systems and cloud types. As quantitative data is sparse, the discussion must be labelled as tentative, but this is not continuously stressed for readability.

In the second part of this chapter we will indicate for which radar wavelengths, cloud types and atmospheric conditions one can theoretically expect coherent particle scatter to be significant (section 6.6). In this section coherent particle scattering is compared in strength to the other two scattering mechanisms. To make the discussion less theoretical, we will refer to some cloud measurements presented in section 6.5. The first part of the chapter (sections 6.2 through to 6.4) serves as a background for this discussion. In section 6.2, the theory of coherent particle scatter will be presented and extended to allow for different slopes of the variance spectrum of the LWC variations. Section 6.3 will give a small literature survey of what is already known about spatial variations in humidity and LWC from in situ measurements. To be able to extend these sparse measurements to other situations, the sources and sinks of the LWC and humidity variations have to be understood; therefore these are discussed in section 6.4. In the last sections conclusions are drawn and some recommendations for further research are made.

6.2 Theory of coherent particle scatter

When particles in some volume have a completely random distribution in space (the so-called Poisson distribution), the average reflected power is simply the sum of the squared amplitudes from the individually reflected waves:

$$\overline{P}_{inc} = \tfrac{1}{2}\sum_n a_n^2 \tag{6.1}$$

In this case the average incoherent particle return ($\overline{P}_{inc}$) is only determined by the amplitude (α_n) of the reflected waves; the phase (or position of the particle relative to the radar) can be ignored in this case. For some particle configurations the interference will be constructive, but for others destructive. For example, in the case of two particles, the reflected power could be 4 times the power of one particle when they are close together and the power could be almost zero when they are about $l/4$ apart as seen by the radar. On average, however, the interference between the waves reflected by the particles can be ignored. When for simplicity we assume that all the N_V particles reflect with the same amplitude (α), the average returned power is $\frac{1}{2}N_V\alpha^2$. For small particles with number density (N) the average radar reflectivity factor is ND^6 (Rayleigh scatter).

When there are spatial correlations in the measurement volume, the phase cannot be ignored. For example, in the extreme case that all particles are confined to a volume much smaller than the wavelength, all amplitudes add up and the returned power is $\frac{1}{2}N_V^2 a^2$, which is much larger than in the incoherent case.

The spatial correlations in clouds can be depicted as lumps of particles and/or voids of particles, with sizes from millimetres to kilometres; they are clearly visible in optically thin clouds, see Fig. 6.1. Because there is structure in clouds (voids and particle lumps), the presence of a particle will enlarge the chance of finding another particle in a volume close by, compared to a remote volume. Such spatial correlations give rise to extra reflections, called coherent particle scatter. Cloud structures with all physical sizes influence the radar backscatter, but mathematically only the Fourier component on a scale of $\lambda/2$ is taken into account. When in the remainder of this chapter variations at a certain scale are mentioned, the Fourier component at this scale is meant.

The radar backscatter for a cloud volume with droplets will be both coherent and incoherent. If we assume a cloud with a mono-disperse drop size distribution with diameter (D) in which the particle mass variations are transported from large scales to small scales by isotropic homogeneous turbulence, the radar backscatter is given by [chapter 5]:

$$Z = ND^6 + 4.2\times10^{-3} b^2 L_0^{-2/3} N^2 D^6 l^{11/3} \tag{6.2}$$

Figure 6.1. Clouds have spatial structures on many different scales. The Liquid Water Content variations are clearly visible in this optically thin cloud. These structures can give strong radar reflections.

with N the ensemble average particle number density, L_0 the outer scale length of the inertial subrange of isotropic homogeneous turbulence, and l the radar wavelength. The first term is the incoherent backscatter and the second term the coherent backscatter; for both Rayleigh scatter is assumed. The standard deviation of the spatial Liquid Water Content (LWC) variations is assumed to be a fraction (b) of the total LWC.

The derivation of Eq. (6.2) consists of two steps. 1) Relate the refractive index variations to the liquid water variations. 2) Relate the radar reflectivity to the spatial variations in the refractive index. The treatment of the derivation will be kept short in this chapter, as chapter 5 already discussed it at length. New in this derivation is that we allow the slope of the LWC variance spectrum to assume various values.

Step 1. In Van de Hulst (1981) the refractive index (n) of air with many small spheres is formulated as:

$$n = 1 + \frac{p}{4} KD^3 N \tag{6.3}$$

with $K = (\varepsilon_r - 1)(\varepsilon_r + 2)^{-1}$, a constant that is determined by the relative permittivity of the particles (ε_r); the absorption is neglected. Equation (6.3) is valid if the second term on the right-hand side is small compared to unity, and when the particles are far apart compared to their size, but close together compared to the wavelength. These assumptions are true for a homogeneous cloud and should also hold for the small spatial LWC variations considered in this thesis. For mm-waves this treatment of the discrete particles as a continuous refractive index is not completely justified.

Assuming that the standard deviation of the variations is a fraction of the mean LWC, i.e. $\sigma_{LWC} = \beta \cdot LWC$, or $\mathrm{var}(ND^3) = \beta^2 (ND^3)^2$, one can write:

$$\mathrm{var}\, n = \frac{\pi^2}{16} |K|^2 \, \mathrm{var}(ND^3) = \frac{\pi^2}{16} |K|^2 \, \beta^2 N^2 D^6 \tag{6.4}$$

This variance in refractive index is only the variance of the continuous refractive index field. The variance due to the discrete nature of the droplets is not taken into account.

Step 2. The radar backscatter is determined by the energy of the three-dimensional power density spectrum ($\Phi_n(\boldsymbol{\kappa})$). The backscatter is proportional to the power in a small spectral band around half the radar wavelength in the direction ($\hat{\mathbf{k}}$) of the radar beam. Note that variations at scales larger than $\lambda/2$ can also contribute when they are not parallel to the radar beam, as the projection on the unit vector $\hat{\mathbf{k}}$ is the variable of interest. Following Ottersten (1969) we assume that the spatial variance spectrum integrated over the entire wave number (κ) space is equal to the total spatial variance of the refractive index (var n). To compute this three-dimensional power density integral, an assumption has to be made about the shape of the power density spectrum. A common assumption is that the energy spectrum of the LWC variations follows the well-known −5/3 law for homogeneous isotropic turbulence in the inertial subrange.

Slopes different from −5/3 have been measured in clouds, see section 6.3. That is why an equation for coherent particle scatter for slopes between −1 and −3 will be derived here. According to Tatarski (1961) the three-dimensional spectral density ($\Phi(\kappa)$) for isotropic turbulence spectrum is given by:

$$\Phi(\kappa) = \frac{\Gamma(p+1)}{4\pi^2} \sin\left(\frac{\pi(p-1)}{2}\right) C_n^2 \kappa^{-(p+2)} \tag{6.5}$$

with $\Gamma(..)$ the gamma function, $-p$ the slope of the (LWC) variance spectrum. The structure constant of the refractive index (C_n^2) is a measure of the total amount of refractive index variations per unit volume. The function is only defined for $1<p<3$. For a slope in k-space with $p<1$, the LWC field in physical space will be stationary, but discontinuous. For slopes with $p>1$, the LWC field will be continuous but non-

stationary. However, the increments $[x(x+r)-x(x)]$, which are needed to calculate a structure function, are stationary as long as $p<3$ (Davis, 1996).

The relation between the variations in k-space and the physical space is given by:

$$\int_{-\infty}^{\infty} f(\mathrm{k})d\mathrm{k} = \mathrm{var}\, n \tag{6.6}$$

The largest scale and the smallest scale of the inertial subrange are designated by L_0 and ℓ_0, respectively. In the inertial subrange the above integral can be computed by using Eq. (6.5) and by assuming that there are no variations at scales above L_0 or below ℓ_0. C_n^2 is then given by:

$$C_n^2 = \frac{p-1}{2\Gamma(p+1)\sin\left(p\,(p-1)/2\right)}\frac{(2p)^p}{\left(L_0^{p-1}-\ell_0^{p-1}\right)^{-1}}\,\mathrm{var}\, n \tag{6.7}$$

In clouds there will also be variations at scales above L_0. The comparison between measurements and calculations will be most accurate when these variations at large scales are removed from van n, e.g. by choosing some L_0 in the inertial subrange and only using the variance of the scales smaller than L_0. The relation between C_n^2 and the radar reflectivity can be if the expression,

$$h = \frac{p^2}{2}k^4 j\,(k) \tag{6.8}$$

from Ottersten (1969) is combined with Eq. (6.5):

$$h = \frac{\Gamma(p+1)}{8}\sin(p\,(p-1)/2)k^{-p+2}C_n^2 \tag{6.9}$$

Combining the above with Eq. (6.7) and substituting k by $4\pi\lambda^{-1}$ (the length scale of interest is $l/2 = 2p/k$) yields the radar reflectivity as a function of var n:

$$h = \frac{(p-1)p^2}{2^p}\left(L_0^{p-1}-\ell_0^{p-1}\right)^{-1} l^{\,p-2}\,\mathrm{var}\, n \tag{6.10}$$

The radar reflectivity factor is defined by:

$$Z = \frac{l^4}{p^5\,|K|^2}h \tag{6.11}$$

Finally, by combining (6.4), (6.10), and (6.11), we find the radar reflectivity factor for coherent particle scatter for a variance spectrum with $1<p<3$:

$$Z = \frac{p-1}{16p\;2^p}(L_0^{p-1}-\ell_0^{p-1})^{-1}\,l^{\,p+2}N^2 b^{\,2}D^6 \tag{6.12}$$

which will reduce to the second term on the right-hand side of Eq. (6.2) for p=5/3 and $\ell_0 << L_0$. For most slopes the term with the inner scale (ℓ_0) can be ignored, as the outer scale (L_0) is normally much bigger. However for p→1 the inner scale will become increasingly important.

6.2.1 Coherent and incoherent particle scatter

There are two ways to distinguish coherent from incoherent scatter. The first method uses the difference in wavelength dependence of the coherent and incoherent backscatter. The incoherently reflected power from droplets strongly depends on the wavelength, whereas the coherent backscatter from turbulent variations is less wavelength dependent. The radar reflectivity factor corrects for the incoherent wavelength dependence. Therefore the radar reflectivity factor of a coherently scattering volume becomes wavelength dependent, while the radar reflectivity factor of an incoherently scattering volume is the same for two radars with different wavelengths. The incoherent radar reflection is given by:

$$Z = ND^6 \tag{6.13}$$

For a coherently scattering volume the radar reflectivity factor measured by two radars differs by a factor. For a given slope of the variance energy spectrum, this factor depends on the ratio of the two wavelengths,

$$d = \frac{Z_{coh,1}}{Z_{coh,2}} = \left(\frac{l_1}{l_2} \right)^{p+2} \tag{6.14}$$

For example, the difference in radar reflectivity factor between a 10-cm and a 3-cm radar is 19 dB if the slope ($-p$) of the spectrum is −5/3. Details can be found in, e.g., appendix A of Knight and Miller (1998). A disadvantage of this dual-wavelength method is that the slope of the energy spectrum has to be known accurately. There are indications that the −5/3 law is not always valid, see section 6.6.1 Using for one of the radars a very small wavelength, which will only see incoherent scatter, could circumvent this.

Another method is to look at the angular dependence of forward scatter using a bi-static radar. For radar scatter under an angle, the effective wave number (κ) is given by [Gossard and Strauch, 1980]:

$$k = 2k \sin(q/2) \tag{6.15}$$

with k the absolute wave number of the transmitted wave, and θ the angle between the transmitted and scattered wave (θ=0 for forward scatter). Incoherent scatter does not depend on the azimuth for vertically polarised radio waves, whereas coherent scatter will change as given by Eq. (6.15). The advantage of this method is that the

coherent scatter can be determined for a range of wave number values and it becomes possible to estimate the slope of the variance spectrum within this range. However, because scanning is necessary to determine the angular dependence, this method can only be used for homogeneous clouds.

6.2.2 Coherent air and coherent particle scatter

In general it is not possible to distinguish coherent particle scatter from coherent air scatter by measuring with a radar. In some special cases it can be possible to indicate which of these scattering mechanisms dominates the radar return. For example, a correlation between the incoherent particle scatter (the reflections from a short-wavelength radar) and the coherent scatter (long wavelength) is an indication that the coherent scatter is from particles and not from the air, see Chapter 5. Such a correlation has been observed in S- and X-band measurements of cumulus clouds.

However, there does not have to be a correlation between incoherent and coherent particle scatter. First of all, if a correlation is to become noticeable, one variable has to vary much more (the droplet diameter in the case of this cumulus measurement, due to condensational growth) than the other variables in Eq. (6.12).

Secondly, the drop size distribution has to be well behaved: There has to be a stable relation between the smaller and the larger particles of the drop size distribution, as the coherent particle scatter is more sensitive to small drops and incoherent scatter to large drops. This is due to the fact that coherent particle scatter in clouds is proportional to N^2D^6 (or LWC^2) and the incoherent particle scatter to ND^6, and generally there are more small particles. For example, for drizzling clouds the correlation between coherent and incoherent particle scatter is likely to be poor.

For cumulus clouds there is a strong relation between the smaller drops and the larger drops: based on in situ measured (FSSP) drop size spectra Paluch et al. (1995) estimate that using the incoherent particle scatter (sensitive to the larger drops) the LWC (sensitive to the smaller drops) can be estimated with an error of just 13 %. In stratocumulus clouds the relation between LWC and the incoherent particle scatter can be very weak [Fox and Illingworth, 1997; De Wit et al., 1999]. For these clouds the correlation between incoherent and coherent particle scatter is also likely to be poor.

In some cases coherent air scatter can be distinguished from particle scatter (either coherent or incoherent) based on the Doppler velocity, see e.g. Cohn et al. (1995) who are able to distinguish between coherent air scatter and reflections from rain. Other instruments can help to determine the dominant coherent scattering mechanism. An example is using a lidar to ascertain whether particles are present in the first place. Coherent air scatter in clouds will be strongest (or weakest) when the air outside the cloud is relatively dry (or humid). An instrument capable of measuring humidity (radiosonde, microwave radiometer, etc.) can therefore be of help.

6.3 Measured spatial variations

The magnitude of the spatial variations in LWC determines the strength of coherent particle scatter, while the spatial humidity variations determine the coherent air scatter. In their comparison of coherent particle and coherent air scatter Gossard and Strauch (1981) state that within a cloud in steady-state at saturation with no precipitation removing water from the cloud and minimal entrainment it seems reasonable to assume that the variance of humidity is about the same as that of the LWC. This is a logical assumption for the *temporal* variance of an isolated cloud volume as a change in humidity must result in an equal change in LWC. The radar backscatter is determined by the *spatial* variance, however. It is theoretically possible to change the spatial variance of the LWC without affecting the spatial humidity variance. Furthermore, for many (parts of) clouds the assumption of minimal entrainment will not be valid. Therefore, one will have to look for the sources and sinks of spatial variations to estimate the magnitude of humidity and LWC variations (see section 6.4), or directly use the measurements of those variations. That is why in this section some of the literature on in situ measured spatial variations will be reviewed.

In literature a large set of in situ measurements of spatial variations are described, the latest at very small scales. Often just measurements of spatial variations in *number density* are tested for *statistical* significant deviations from the Poisson statistics. However, for coherent scatter *physically* significant spatial variations in *liquid water content* and *humidity* are of interest. Variations in number density are not readily translated into LWC variations. Furthermore, a volume with statistical significant LWC variations may not have physically significant LWC variations, i.e. give little coherent particle scatter.

Davis et al. (1999) measured spatial LWC variations down to scales of 4 cm with a Particulate Volume Monitor (PVM-100A) probe in broken stratocumulus clouds with embedded towering cumulus clouds as a part of the Southern Oceanic Cloud EXperiment (SOCEX). The average LWC in the cloud is 0.290 ± 0.167 g/m^{-3}, so the relative standard deviation is 58 percent. They find a significant change of the slope (a scale break) of the LWC variance spectrum at scales of 2 to 5 m. At longer scales, the slope is close to $-5/3$ (-1.6 ± 0.1), but at smaller scales there are more variations than expected from the $-5/3$ slope as here the slope is -0.94 ± 0.10. These extra variations at small scales correlate with spikes occurring in the LWC time series (voids or blobs at most a few 4-cm pixels wide). Davis et al. attribute the extra spatial variations below 2 to 5 m to these spikes.

In an earlier article with LWC measurements of stratocumulus from the FIRE87 campaign Davis et al. (1996) also find spikes in some parts of the LWC time series. Other parts are relatively smooth. These measurements with a King probe have a resolution of 5 m. The average relative standard deviation was about 19 %, but it varied highly per measurement; the lowest value found was 5 % and the highest

25 %. The average slope of the LWC variance spectra from all flights was -1.36 ± 0.06, significantly flatter than $-5/3$.

One of the first measurements of cm-scale variations was done by Baker (1992). Measurements of cumulus clouds at all heights were performed with a Forward Scattering Spectroscope Probe (FSSP) with a spatial resolution of about 0.32 mm. Baker tested the variance of the number of droplets relative to the mean. This way he found statistically significant spatial correlations in number density on cm-scales in the majority of cloud penetrations. However, statistically significant variations on all measured scales were only observed in small parts (often near edges) of many clouds and throughout a few clouds.

Malinowski et al. (1994) observed that entrained air contained filaments of cloudy air with droplet concentrations close to those observed in the clouds. Furthermore, they suggest that the distribution of these filaments is anisotropic.

Jameson et al. (1998) performed measurements using the Particle Measurement System (PMS): two-dimensional optical array probes with a resolution of 130 m in a tropical warm precipitating cumulus about 1 km above the cloud base. The main conclusion of these authors is that spatial variations in drop counts are statistically significant from 130 m up to 2 km scales (variance is much larger than the mean). Besides that they also found variations down to 5 cm scales, using the distribution of the interdrop distance.

Korolev and Mazin (1993) have carried out extensive measurements with an FSSP-100 of stratiform clouds (stratus, stratocumulus, altostratus, altocumulus, and nimbostratus). In total 50 cloud with a total length of 1710 km were measured layers on 20 different days. On the basis of this data set they conclude that cloud holes occur most frequently in the vicinity of the upper and lower boundaries of the cloud, but also in parts removed from the upper and lower boundary by hundreds of meters. About 80 percent of these holes was of the smallest size (up to 10 m). On average the holes (defined as volumes with less than 50 percent of the average number density) occupied about 7 percent of the cloud volume. However, this number varies highly: in some clouds it was 20 percent and sometimes no holes were found for dozens of kilometres. Also regions with an increased droplet number concentration were found. However, these were mainly due to the appearance of a large number of small droplets, so these may not be that important for the spatial variations in LWC.

Kozikowska et al. (1984) made a hologram of 22.5 cm^{-3} in fog to measure the three-dimensional droplet distribution on the smallest scales. The distribution of the number density in this one sample is significantly not a Poisson distribution.

Humidity variations have been measured by Politovich and Cooper (1988). They estimate the supersaturation in cumulus clouds with a resolution of 10 m by measuring the vertical velocity (Rosemount 858 gust probe) and the drop size distribution

(FSSP). The supersaturation was estimated to be in the range of −0.5 to 0.5 % for all cloud regions during 147 cloud penetrations of 13 clouds on 8 days. In the entrained regions the standard deviation was below 0.4 % and in the core of the cloud around 0.1 %.

Concluding, measurements of cumulus, stratus clouds and fog with a variety of instruments indicate that non-Poisson distributed droplets occur regularly. However, Poisson distributions are found as well. Especially the presence of spatial variation in the adiabatic cores of cumulus clouds is still under debate, see Grabowski and Vaillancourt (1999) and references therein. The structure of the variations is described as spikes [Davis, 1996] and anisotropic filaments [Malinowski et al., 1994]; the theory of coherent particle scatter may have to be modified to account for such strong variations.

Unfortunately quantitative measurements of spatial LWC variations could only be found for stratocumulus (with embedded cumulus), whereas for some cloud types no measurements of spatial variations could be found at all. Only one indirect measurement of spatial humidity variations was found in literature. No simultaneous measurement of humidity and LWC variations was found in literature. The strength of the coherent backscatter can only be estimated using the available quantitative measurements, which is done in section 6.6.

6.4 Sources and sinks of spatial variations

To be able to extrapolate the sparse measurement data to other cloud types and atmospheric conditions, one needs to know the sources and sinks of these variations. We identify a number of possible sources for spatial variations of LWC.

At the base of the cloud, differences in the condensation level of the air parcels can create variations due to differences in the temperature and humidity of the initial air parcels. Korolev and Mazin (1993) estimate that the variations in the condensation level which are caused by this lie in the order of tens of meters. This fits with their observation that a relatively higher number of cloud holes occur in the lowest 100 m of stratiform clouds compared to the middle of the cloud.

Spatial variations can also be caused by vertical movements in a sub-adiabatic cloud. For a typical stratiform cloud, Korolev and Mazin estimate that a descending movement of 60 m can create a cloud hole.

Spatial LWC variations may also be created by the inertia of the droplets in a turbulent field, often called preferential concentration of droplets, see e.g. Squires and Eaton (1991), Shaw et al. (1998), Vaillancourt (1998) and Pinsky et al. (1999). In a vortex particles are propelled outward by the centrifugal force, so after some time the vortex is particle-free; the particles have moved to quiet areas with low vorticity.

(For an introduction to vortices in turbulence see e.g. the textbook by Frisch (1998) in section 8.9). It is still under discussion whether the right conditions are present in (cumulus) clouds, as realistic modeling of turbulence in clouds is still too difficult. Important unknown factors are the lifetime of the vortices, their volume fraction and the influence of sedimentation due to gravity. Preferential concentration could be an important mechanism as it can also act in the adiabatic cores of clouds.

Entrainment of dry and droplet-free air from outside the cloud is especially important at the cloud top, amongst others due to loss of stability of air parcels by radiative cooling. Entrainment or mixing can also be important at the sides of cumulus clouds. The spatial humidity variations caused by mixing give rise to mantle echoes at the cloud edges on dry days. These mantles can be up to 1 km thick at S-band, see, e.g., Knight and Miller (1998).

When making statements about (the absence of) mixing, one has to remember that an adiabatically ascending air parcel is an idealisation. A parcel always has some heat exchange; whether this is a significant deviation from adiabaticity will depend on the research question. For example, the S-band reflectivity in one of the examples in the paper of Knight and Miller (their Fig. 6) shows a 500 m thick mantle echo caused by coherent air scatter (humidity variations). This coherent air scatter is thought to be caused by *mixing* with environmental air. The X-band reflectivity shows flat echo bases at already a few tens of meters from the cloud edge, however, and these echo bases are interpreted by Knight and Miller as *unmixed* ascent of the cloud air parcel. These two statements do not contradict each other since the amount of mixing to create coherent scatter is probably less than the mixing needed to get a significant decrease in average LWC.

Sinks for LWC variations at large scales are turbulence (which transfers the variations to smaller scales) and a sink for LWC variation at small scales is sedimentation.

Concluding, all the above mechanisms entrainment, parcel differences at cloud base, vertical movements in sub-adiabatic clouds, and preferential concentration depend on the strength of the turbulence. The first three effects become stronger in a more turbulent situation. For preferential concentration the relation with the turbulence strength may be more complex. As mixing with environmental air is an important mechanism at cloud edges and the gradients are high at the top and sides of the clouds, the spatial variations are expected to be largest at these cloud edges. For stratiform clouds this is confirmed by Korolev and Mazin (1993), who state that cloud holes are found more often at cloud tops. For cumulus clouds this is confirmed by the mantle echoes.

Less is known about the sources and sinks of humidity variations in clouds. Sources should be entrainment, the finite relaxation time of evaporation and condensation after the temperature of the parcel has changed due to turbulence or an updraft or

downdraft. Sinks should be turbulence, diffusion and evaporation and condensation. Thus also humidity variations are expected to be largest at the cloud boundaries. Evaporation and condensation are expected to be important sinks of humidity variations in clouds.

In theory it could be possible that a cloud has a lower radar reflectivity than its surroundings when the reflectivity from the surroundings comes from humidity variations. In the case of small fair-weather clouds in the convective boundary layer one may be able to measure such a effect with a windprofiler (for coherent scatter) and a lidar ceilometer (for cloud detection). If this effect were to occur, this would provide evidence that evaporation and condensation are important sinks for humidity variations. Care has to be taken as big clouds will also decrease the coherent air scatter in the boundary layer by reducing the solar flux, however.

6.5 Radar measurements

This section presents some radar cloud measurements in which coherent particle scatter may play a role. They will be used in section 6.6 for a quantitative discussion. There are also strong indications of coherent particle scatter in a dual-wavelength measurement of a smoke plume, see chapter 5.

In a recent article, Knight and Miller (1998) discuss a large number of measurements of developing cumulus clouds, performed with 2 radars: an X-band radar and an S-band radar with wavelengths of 3 and 10 cm, respectively. Most measurements could be explained by using the traditional theory. However, on humid days, the patterns for both radars looked similar, resulting in a correlation between the S- and the X-band reflectivity factors. This correlation is puzzling in cases where the difference in reflectivity factors is not equal to 0 dBZ (for purely incoherent scattering) or 19 dBZ (for purely coherent scattering). In some measurements the X- and S-band reflectivity factors lie on a line with a slope of one, with a typical difference of about 10 dBZ; other offsets have been measured as well. The phenomenon is mostly confined to the core of the reflectivity pattern and its nearby surroundings and to the region near the cloud base.

A similar correlation in a cumulus cloud was measured by Baker et al. (1998), who already speculated that the droplets may scatter coherently. A quantitative explanation for these correlations in cumulus clouds in terms of coherent particle scatter can be found in chapter 5. Knight and Miller also observed cases in which the difference between the reflectivity factors was more than 19 dB (up to 22 dB) in the mantle echo. This indicates that the slope of the humidity spectrum is steeper than $-5/3$. For instance, in the case the difference is 22 dB, the slope is -2.2. Knight and Miller give another possible explanation for the large difference in reflectivity factors: the

spatial variations measured by the X-band may not be in the inertial subrange, but in the dissipation range (below ℓ_0)

By measuring the forward and the backward scattering with two X-band radars Gossard and Strauch (1980) were able to separate coherent from incoherent scatter and to measure the coherent scatter as a function of wave number, see also section 6.2.1. During clear-air situations they found a slope of the energy spectrum of −1.7, near −5/3. However, in a cloudy situation in winter the slope was less steep: −0.9. Unfortunately there is no information on the type of clouds measured and other atmospheric conditions (e.g. humidity outside the clouds). For this measurement the nature of the coherent scatter is unknown.

Gage et al. (1999) have performed 3 weeks of measurements with two windprofilers (wavelengths: 11 and 33 cm) of clouds during the Maritime Continental Thunderstorm EXperiment (MCTEX). For these wavelengths the difference in radar reflectivity factor is 18 dB for coherent scatter from a variance spectrum with a slope of −5/3. In the coherent scatter from clouds at 2 km height, they found that the difference is seldom 18 dB. Most differences are 15 to 16 dB. If this were caused by a flatter slope of the variance spectrum, the slope would be between −1.1 and −1.3. For this measurement it is not clear whether the coherent cloud reflection would come from humidity or LWC variations. Gage et al (1999) speculate that another cause of the 15 dB difference in reflectivity may be a difference in the beam widths of the windprofilers.

During the same campaign an ice cloud was measured with the windprofilers, as reported by Gage et al. (1999) and Ecklund et al. (1999). This ice cloud was observed at a height range of 6 to 18 km. The difference in radar reflectivity factor is zero; only Rayleigh scatter is present in this cloud.

A measurement during the Dutch CLARA (CLouds And Radiation) campaigns [Van Lammeren et al., 1999] of a stratocumulus cloud is shown in Fig. 6.2a. The radar reflectivity factor is measured by the 9-cm wavelength Delft Atmospheric Research Radar (DARR). A histogram of the maximum values of the reflectivity profiles is shown in Fig. 6.2b. Values above −20 dBZ are not uncommon, whereas in situ drop size distributions measured with an FSSP-100 never produce values above −25 dBZ for incoherent droplet scatter. The number density is in the order of 500 cm^{-3} and the diameter at the height of the radar reflections in the order of 10 μm. The large difference between the incoherent scatter calculated from the FSSP measurements and the measured radar reflectivity suggests that the scatter is enhanced by coherent scattering by humidity or droplets.

One can not draw a definite conclusion though, as a few large particles can enhance the radar reflectivity a lot [Fox and Illingworth, 1997; De Wit et al., 1999], whereas the FSSP may miss these particles due to the small sampling volume and the small maximum drop size. The aeroplane also did not fly at the height where the maximum reflectivity values occur at the time the highest values occurred. Still the

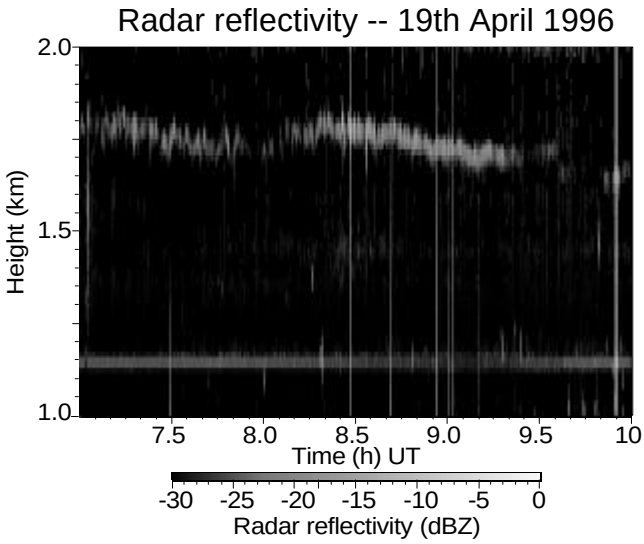

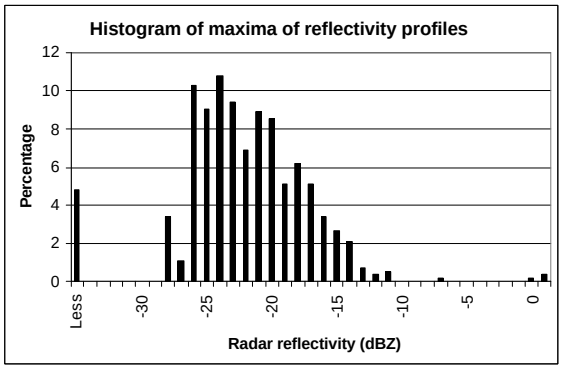

Figure 6.2. Measurement of stratocumulus cloud (6.2a) made on the 19th of April 1996 with the Delft Atmospheric Research Radar (DARR), a 9-cm FM-CW radar. The histogram (6.2b) shows the maximum values of the vertical radar reflectivity profiles between 8 and 9:30 hrs UT of the stratocumulus cloud shown in Fig. 6.2a. The perfectly straight vertical and horizontal lines should be ignored; they are not cloud related.

difference in the radar reflectivity values is intriguing, especially as coherent particle scatter at S-band in stratocumulus is theoretically likely to dominate incoherent scatter, see section 6.6.3.

6.6 Discussion of the measurements

In this section the strength of coherent particle scatter, coherent air scatter and incoherent particle scatter will be calculated for various values of the variables involved. As the slope of the variance spectrum is a complex variable, it will first be discussed in section 6.6.1. The radar measurements from the previous section will be discussed as special cases. The in situ measurements of section 6.3 are used as a reference for the characteristics of the spatial variations.

6.6.1 Slope of variance spectrum

Assuming fully developed isotropic turbulence, one gets a slope of −5/3 in the inertial subrange if the sources of the variations act on scales larger than the outer scale (L_0) and the sinks act on scales smaller than the inner scale (ℓ_0). For a passive *conservative* additive the slope of the variance spectrum of the additive is the same as the slope of the turbulent energy spectrum [Tatarski, 1961]. However, both the amount of water vapour and liquid water are not conservative in clouds. One can expect the slope of the humidity or LWC variance spectrum to become more flat (steep) if there is an additional source (sink) of variations within the inertial subrange. The various slopes that have been measured in situ (see section 6.3) or by radar (see section 6.5) are summarised in Table 6.1.

There is some evidence for a steeper slope for humidity variations and a flatter slope for LWC variations; both have been measured and there are mechanisms that may explain it. However, the amount of data is much too sparse for general conclusions, especially for extrapolations to different cloud types and atmospheric conditions.

The deviations in slope from −5/3 are important for the strength of coherent particle scatter compared to the other scattering mechanisms, as will be shown in

Cloud type	Slope		Measurement method	Source
Stratocumulus	−0.94 ± 0.10	LWC	In situ, at scales below 5 m	Davis et al. (1999)
Stratocumulus	−1.6 ± 0.1	LWC	In situ, at scales above 5 m	Davis et al. (1999)
Stratocumulus	−1.36±0.06	LWC	In situ	Davis et al. (1996)
Cumulus	−2.2	Humidity	Dual-wavelength radar	Knight and Miller (1998)
Winter clouds	−0.9	Unknown	Forward scattering radar	Gossard and Strauch (1981)
Low level clouds	−1.1 to −1.3	Unknown	Dual-wavelength radar at 2 km	Gage et al. (1999)

Table 6.1. Slopes of the variance spectra in clouds.

section 6.6.2 for the coherent air scatter and in section 6.6.3 for incoherent scatter. For understanding the coherent scatter measurements with radar, the slope of the variance spectra must be measured preferably simultaneous in situ humidity and LWC measurements and the underlying mechanisms that influence the slope must be well understood.

6.6.2 Coherent particle scatter and coherent air scatter

Gossard and Strauch (1983) calculated that if the spatial variance of the water vapour content is equal to the spatial variance of the liquid water content, the radar reflectivity due to the humidity variations should be about 28 times larger. The quantitative relations are:

$$\begin{aligned} 10^{12} \cdot \mathrm{var}\, n_L &= 2.09 \cdot \mathrm{var}\, L \\ 10^{12} \cdot \mathrm{var}\, n_V &= 58.5 \cdot \mathrm{var}\, V \end{aligned} \qquad (6.16)$$

with, respectively, var n_L and var n_V as the variance of the refractive index due to Liquid water variations (var L) and water Vapour variations (var V). In other words, if the coherent particle scatter is to dominate the coherent air scatter, the standard deviation of the spatial LWC variations should be at least 5.3 times as large as the standard deviation of the spatial humidity variation. For the above statements about the radar backscatter the slopes of both variance spectra are assumed to be equal.

Using the measurement of spatial humidity variations by Politovich and Cooper (1988) we will show that coherent particle scatter can dominate coherent air scatter for cumulus clouds. The regions giving a high correlation between the S- and the X-band in the article by Knight and Miller (1998) are about 2 km above cloud base. An *adiabatic* cloud with a temperature of 25 degrees Celsius and a pressure of 930 mb at cloud base will have a water vapour content of about 17 g m^{-3} and a liquid water content of about 6 g m^{-3} at 2 km above cloud base. These cloud-base temperatures were observed by Paluch et al. (1996), who measured them during the CaPE-1991; the Knight and Miller radar measurements are from the same campaign. As in the region with the correlations in radar reflectivity the absolute amount of liquid water and water vapour are about equal, one can simply compare the relative variations.

The relative standard deviations in the spatial humidity variations measured by Politovich and Cooper (1988) are: 0.4 % in 80 percent entrained air and 0.1 % in the core of cumulus clouds. If the coherent particle scatter is to dominate coherent air scatter, the standard deviations of the spatial LWC variations should be 5.3 times bigger, so above 6 % for the entrained region and above 1.5 % in the core of cumulus clouds. These values are low compared to the measured LWC variations (5 to 58 % in stratocumulus) and compared to the LWC variations that are needed if co-

herent scatter is to be stronger than incoherent scatter at S-band. Furthermore, to explain the dual-wavelength radar measurements of Knight and Miller (1998), we needed about 25 % LWC variations [chapter 5]. Lower in the cloud the ratio of water vapour content and liquid water content will be higher, so coherent *air* scatter will probably be more important near the cloud base. Therefore it is likely that the scatter by the waterdroplets (either coherent of incoherent) should dominate coherent air scatter throughout cumulus clouds except close to the cloud base. The assumption made then is that the relative LWC variations in cumulus and stratocumulus are in the same order of magnitude.

In stratocumulus the LWC is generally much lower than near the top of large cumulus clouds. When the standard deviation in LWC is 0.167 g/m^{-3} as in Davis (1999), the standard deviation in humidity should be 0.03 g/m^{-3} to get the same amount of scattering from both mechanisms. This corresponds to a humidity of 7.5 g/m^{-3} (dew-point temperature: T_d = 6 °C) with 0.4 % standard deviation or to a humidity of 30 g/m^{-3} (T_d = 30 °C) with 0.1 % standard deviation. As these humidity values are of a natural order of magnitude, and no in situ humidity variation measurements are available in stratiform clouds, a conclusion about these clouds cannot yet be drawn. Simultaneous measurements of humidity and LWC variations are needed.

In the above calculations the slope of the LWC and humidity variations are assumed to be equal. When this is not the case, the results can be drastically different. Assuming that $\ell_0 << L_0$ one can derive using Eq. (6.10) that:

$$\frac{h_L}{h_V} = \frac{p_L - 1}{p_V - 1} 2^{-p_L + p_V} L_0^{-p_L + p_V} l^{p_L - p_V} \frac{\operatorname{var} n_L}{\operatorname{var} n_V} \tag{6.17}$$

with η_L and η_V the radar reflectivity due to LWC variations and humidity variations, respectively, and $-p_L$ and $-p_V$ the slopes of the LWC and humidity variance spectra, respectively. Using Eq. (6.16) this becomes:

$$\frac{h_L}{h_V} = \frac{p_L - 1}{p_V - 1} 2^{-p_L + p_V} L_0^{-p_L + p_V} l^{p_L - p_V} \frac{\operatorname{var} L}{28 \operatorname{var} V} \tag{6.18}$$

In Fig. 6.3 η_L and η_V are compared for various slopes and wavelengths for identical variance of humidity and LWC and L_0 = 10 m. For a larger value of L_0 the differences will be larger. In Fig. 6.3 one can see that for equal slopes the coherent air scatter (drawn lines) is 15 dB larger than the coherent particle scatter (dashed lines), as expressed by Eq. (6.16). When the slope of the humidity variations is steeper than the one of the LWC variation the lines can cross and the LWC variation can reflect more power than the humidity variations.

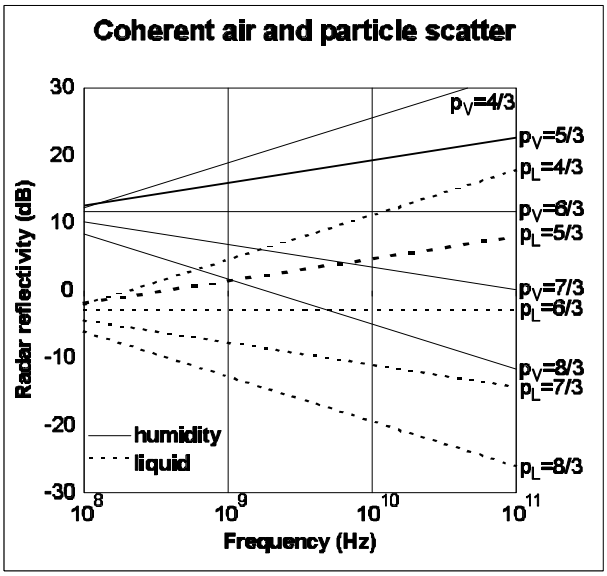

Figure 6.3. Calculation of the strength of coherent air and coherent particle scatter for different slopes of the humidity and LWC variance spectrum using Eq. (6.10) and (6.16). The dashed line is the radar reflectivity from LWC variations and the drawn line from the humidity variations. The variances in humidity and LWC are equal, and L_0 is 10 m.

As an example one can calculate (or read from Fig. 6.3) the radar reflectivity for equal variations in LWC and humidity (var L = var V), and a slope of the humidity variations ($-p_V$) of −2.2 and a slope of the LWC variations ($-p_L$) of −1.36 (see section 6.6.1 for the values of the slopes). For an S-band radar (λ=0.1 m) and L_0=10 m, the radar reflectivity due to LWC variations will now be almost equal to the radar reflectivity due to humidity variations, instead of 28 times smaller. These are preliminary calculations as the value of the outer scale (L_0) is important, but not well known, and the data on the slopes is insufficient. However, the calculations do show that the slope of the spectra can be a factor that may not be ignored when comparing coherent air and coherent particle scatter.

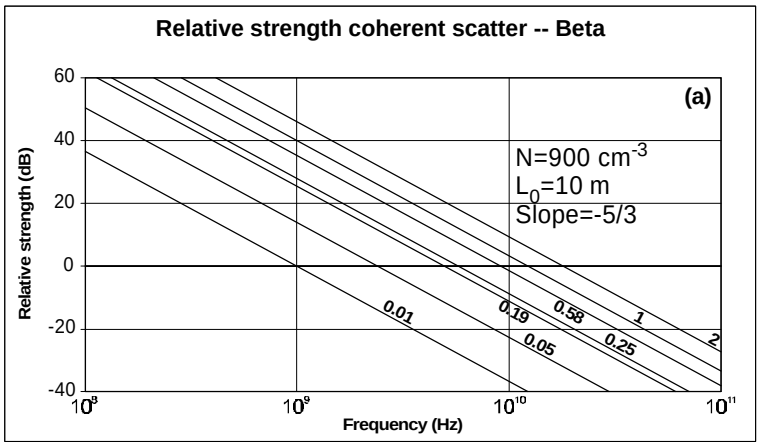

Figure 6.4a-b. Plots of the relative strength of coherent particle scatter compared to incoherent particle scatter as a function of radar frequency as calculated by Eq. (6.12). Fig. 6.4a shows the influence of the relative standard deviation of the LWC. Fig. 6.4b shows the influence of particle number density. See next page for Figures 6.4c and 6.4d.

6.6.3 Coherent and incoherent particle scatter

To see how important incoherent scatter is compared to coherent particle scatter, one has to compare the two terms in Eq. (6.2). Chapter 5, using values from literature, already showed that coherent particle scatter can dominate incoherent particle scatter for the cumulus cloud measurement by Knight and Miller (1998). Knight and Miller measured 10 dB more (coherent) backscatter at S-band than at X-band. To

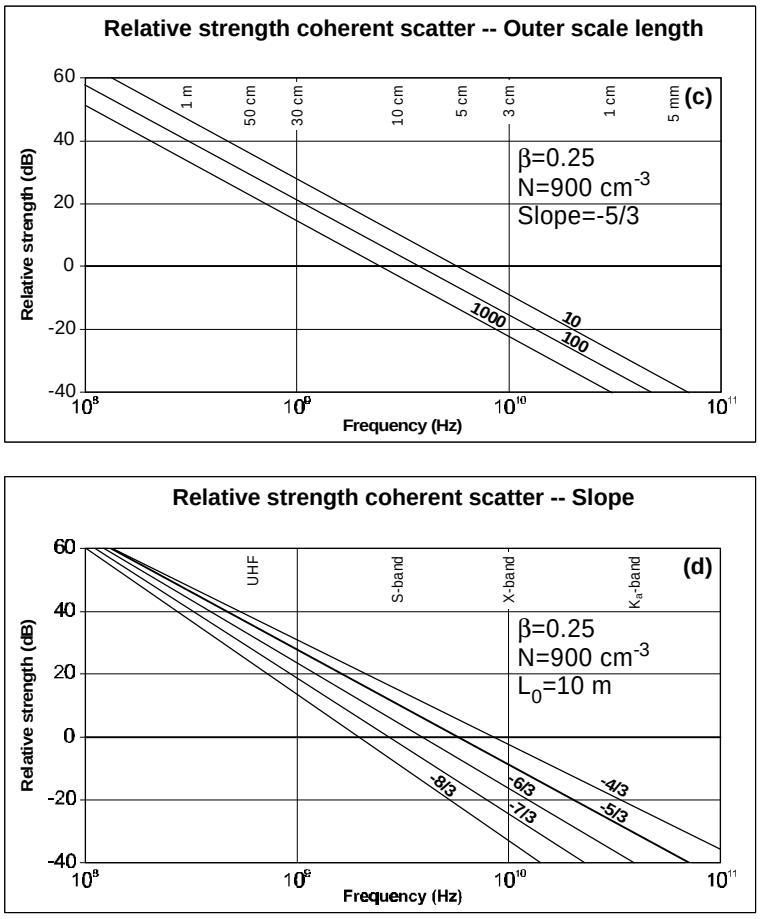

Figure 6.4c-d. Plots of the relative strength of coherent particle scatter compared to incoherent particle scatter as a function of radar frequency as calculated by Eq. (6.12). Figure 6.4c shows the relation for some values of the outer scale of the inertial subrange L_0. The slope dependence is shown in Fig. 6.4d. Figure 6.4a and 6.4b are on previous page.

explain this with coherent particle scatter chapter assumed the values: L_0 = 10 m (from VanZandt et al. (1978)), ℓ_0=0, $N = 800 \cdot 10^6$ m^{-3} (from Paluch et al. (1996)), λ = 0.1 m, and a slope of -5/3, to arrive at a relative spatial standard deviation of b = 0.25. With a flatter slope (p=1.36) and the other variables the same, b would have to be 0.14.

To explain the S-band radar reflectivity factor values of a stratocumulus cloud (Fig. 6.2) by coherent particle scatter one can use the number density

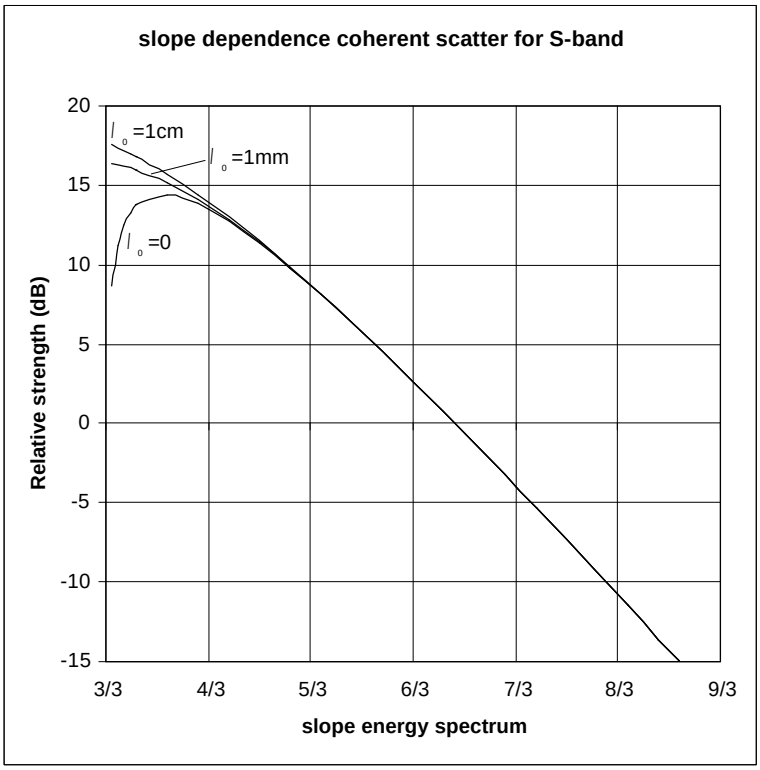

Figure 6.5. The relative strength of coherent particle scatter compared to incoherent particle scatter as a function of the slope of the variance spectrum for an S-band radar, using Eq. (6.12). The figure shows that for small slopes the inner scale of the inertial subrange becomes important. The relation is plotted for three inner scales: 0, 1 mm and 1 cm. Other variables used are L_0=10 m, b=0.25, N=900 cm^{-3}, λ=9 cm, and p=5/3.

(N=500·10^6 m^{-3}) and diameter (D=10 μm) from the FSSP measurements. Then, using the values L_0 = 10 m, ℓ_0=0, λ = 0.09 m, and p=5/3, one will get -20 dBZ scatter with b = 0.55 and -10 dBZ with b = 1.75. With a flatter slope (p=1.36) and the other variables the same, b would have to be 0.33 to get -20 dBZ and 1.03 to get -10 dBZ.

Unfortunately, it is not possible to calculate the backscatter for a slope with p=0.9, but b should be smaller in that case. The relative spatial standard deviations (b) calculated above are high, but may not be unreasonable for a thin cloud, which can be highly entrained.

To investigate this relation for other situations we illustrate the influence of the variables in Eq. (6.2) in a few graphs. Fig. 6.4a shows the relative strength of coherent particle scatter compared to incoherent particle scatter for different values of the relative standard deviation of spatial LWC (b). The other values are for a cumulus cloud case: L_0 = 10 m, $N = 900 \cdot 10^6$ m^{-3}. The values for b are taken from the previous discussion, including some more extreme examples. The high values may occur at cloud boundaries and the low ones in a quiet cloud.

In Fig. 6.4b the relative strength of coherent particle scatter compared to incoherent particle scatter is investigated in relation to the number density (N), where the other values are: L_0 = 10 m, b = 0.25. Measured number densities from literature are summarised in Table 6.2; there is a considerable spread in the naturally occurring number densities. A number density of 1000 cm^{-3} is a high value for cumulus, 200 to 500 cm^{-3} is representative for continental stratus clouds, the value of 10 cm^{-3} corresponds to some ice clouds.

That the outer length scale is relatively less important can be seen in Fig. 6.4c. The other values are taken to be: $N = 900 \cdot 10^6$ m^{-3}, b = 0.25. The value for the outer scale is uncertain. VanZandt et al. (1978) used 10 m and Crane (1980) estimated it to be 10-100 m in the free atmosphere. L_0 is largest in turbulent regions with low hydrostatic stability [Gage, 1999]. We included this graph with L_0 as independent variable to show that the spread is not very large compared to the other variables.

The relative strength of coherent particle scatter compared to incoherent particle scatter is plotted in Fig. 6.4d as a function of the slope (p) using Eq. (6.12). The

Cloud type	N (cm^{-3})	Comment	Source
water clouds			
Cumulus	800-900	Near cloud base.	Paluch et al. (1996)
Continental Cumulus	500-800	30 minutes of data in Montana.	Politovich and Cooper (1998)
Continental stratocumulus	200-500	One measurement.	Korolev and Mazin (1992)
Continental stratus	347	About 1.5 hrs of data.	Sassen et al. (1999)
Coastal stratus	75-150	One measurement.	Korolev and Mazin (1992)
Fog	50	One volume of 22.5 cm-3.	Kozikowska et al. (1984)
Fog	1 to few hundred		Pruppacher and Klett (1997)
ice clouds			
Altostratus	Up to 10		Pruppacher and Klett (1997)
Alto stratus Alto cumulus	75	One measurement.	Korolev and Mazin (1992)
Cirrus	0.05 to 0.5		Pruppacher and Klett (1997)
Cirrus	Up to 0.2	Model, highest N at top.	Sassen and Khvorostyanov (1998
Ice fog	100-200		Pruppacher and Klett (1997)

Table 6.2. Number densities found in clouds.

other values are taken to be: $b = 0.25$, $L_0 = 10$ m, $\ell_0 = 0$, $N = 900 \cdot 10^6$ m^{-3}. The influence of the slope will become stronger when a larger outer scale is chosen. Unfortunately, it is not possible to draw a line in the figure for the slope of −0.9 found by Davis et al. (1999), as Eq. (6.12) is only valid for $1<p<3$. Furthermore, for slopes between 1 and 1.3 the inner scale of the inertial subrange becomes important, and may no longer be neglected. This can be seen in Fig. 6.5, where the relative strength of coherent to incoherent particle scatter at S-band is plotted as a function of the slopes between 1 and 3. For slopes close to 1 a large part of the variance is distributed at very small scales when the inner scale is put to zero, thus reducing the variance at cm-scales.

Concluding, for an X-band radar, coherent particle scatter can dominate only for the highest values of b and number densities. For mm-wave radars coherent particle scatter is not likely, although given the uncertainty in the variables (especially b and p) it cannot be ruled out. For windprofilers coherent particle scatter will normally dominate incoherent particle scatter. For typical number densities and relative LWC variations in stratocumulus clouds, coherent particle scatter can dominate incoherent scatter for an S-band radar. Given the typical number densities in ice clouds one may need a windprofiler to have coherent scatter dominating. However, recently Baker et al. (2000) presented measurements of very strong spatial structures in ice clouds. They were only seen for the small particles. If there would be no large particles present, these spatial structures seen in the small crystals would highly likely produce coherent scattering as the spatial standard deviation was a few times the mean IWC. When the slope is flatter than −5/3, which may occur as indicated by measurements, this will make coherent particle scatter several dBs stronger at the radar wavelengths. Given the poor present state of knowledge the above conclusion may have to be modified in the future.

6.7 Summary and conclusions

This chapter explored the possibility of significant coherent particle scatter in clouds. Measurements in literature have shown significant spatial variations in liquid water content and humidity in stratus, stratocumulus and cumulus clouds. Unfortunately, quantitative measurements of spatial LWC variations and the slope of the variance spectrum are only available for stratocumulus (with embedded cumulus). Quantitative spatial humidity measurements exist only for cumulus clouds.

Dual-wavelength radar measurements of cumulus clouds show signs of coherent particle scatter at S-band. Radar measurements with a 9-cm wavelength of stratocumulus show some indications of coherent scattering. Furthermore, there is evidence from dual-wavelength measurements that the slope of the humidity spectrum can be

steeper and from in situ measurements that the LWC spectrum can be flatter than the standard value of −5/3, which can be very important for the radar reflectivity.

Theoretical calculations show that coherent particle scatter can dominate coherent air scatter in the top part of cumulus clouds. In stratiform clouds one cannot say whether coherent particle scatter or coherent air scatter is strongest given the large margin of error; simultaneous measurements of humidity and LWC variations will have to be made to determine which mechanisms will dominate. If possible deviations from the −5/3 slope of the variance spectra of humidity and LWC are taken into account, it is possible that coherent particle scatter is stronger than coherent air scatter when the total variance of the humidity and LWC are equal. This contradicts previous calculations with equal slopes, which indicated that coherent particle scatter should be insignificant for equal variations in humidity and LWC.

Incoherent particle scatter should theoretically dominate coherent particle scatter for a mm-wave radar. Which kind of scatter dominates for a cm-wave radar will depend on the cloud type and atmospheric conditions. For a dm-wave radar coherent particle scatter will almost always be more important than incoherent scatter. For an S-band radar coherent particle scatter of stratocumulus clouds can be significant compared to incoherent scatter. However, there is no reliable estimate of the relative strength of coherent air scatter for these types of clouds. When the slope is flatter than −5/3, as is indicated by measurements, coherent particle scatter will be several dBs stronger at wavelengths below 1 m.

6.8 Recommendations and outlook

Since until now not much attention was given to coherent particle scatter, still many questions remain. To test the theory of coherent particle scatter, simultaneous measurements of LWC and humidity variations should be compared to radar measurements of coherent scatter. Experiments on cumulus clouds similar to those of Knight and Miller but with a mm-wave radar as smallest wavelength or a bi-static forward scattering radar setup could confirm the theory if similar results are produced.

To develop the theory further, small-scale in situ measurements should be made of humidity, LWC and temperature spectra, both of the total variance and the slopes. These measurements should preferably be done in the same volume, so that the covariances at small scales can be determined as well. Measurements of the LWC and humidity spectra should be made for a range of different cloud types to determine which type of coherent scatter is important for which type of cloud. These spectra

should be measured at scales close to the radar wavelength, to reduce problems with the slope of the variance spectra. A theoretical expression for coherent particle scatter for LWC spectra with a slope flatter than −1 should be developed, since −0.9 has been observed.

If coherent particle scatter is often significant in clouds, this may open fascinating new areas for atmospheric radar research. Below some possibilities are given.

It may be possible to develop a method that uses the coherent particle scatter to measure the LWC of clouds. Such a method would have less problems with big drops in the cloud than methods using incoherent scatter. This method will only work if the big drops are not fully dominating the total reflection so much that the coherent term is too difficult to measure. Furthermore, one should be sure that coherent air scatter can be ignored for the cloud studied. The amount of spatial variations is unknown, thus the coherent scatter cannot be used directly. However, a method analogous to the method of Frisch et al (1995) may be applicable: to use a radiometer to restrain the total amount of liquid water in the column (LWP). An assumption about the shape of the relative variation (b) profile in the cloud would then be needed. For a thin cloud it may be allowed to assume b is constant with height.

In a similar way, the difference in the sensitivity of coherent and incoherent particle scatter to particle size may be usable for cloud boundary measurements during rain. Venema et al. (1999) showed with radar and lidar measurements that the radar reflectivity of clouds is insignificant compared to the radar reflectivity of even very light precipitation, which makes cloud boundary measurements using the *total* radar reflectivity impossible during rain. However by carrying out high-Doppler resolution measurements with two wavelengths it may be possible to distinguish between reflections of rain and cloud in a certain velocity and height cell. The cloud particles have a smaller velocity and may scatter a bit stronger (in dBZ) for the longest wavelength compared to the shortest. The precipitation will scatter equally in the Rayleigh domain and fall faster than the cloud droplets. Using only velocity information one can get difficulties with up- and downdrafts.

A radar with a long wavelength may detect some clouds more easily than a radar with a short wavelength of similar sensitivity expressed in radar reflectivity factor.

Radar measurements might contribute to the research on LWC and humidity variations, which are important for understanding the broadening of the drop size distribution during the development of cumulus clouds and consequently for warm-rain formation. The LWC can be determined by a radar in combination with other remote sensing instruments [Erkelens et al., 1999a; Boers et al., 1999; Frisch et al., 1995]. Given the LWC, the measured coherent particle reflection can then be used to estimate the magnitude of the spatial variations at scales close to half the radar wavelength.

References

Baker, B.A., P. Lawson, and C.G. Schmitt. Clumpy Cirrus. *Proc. 13th Int. Conf. on Clouds and Precipitation*. Reno, Nevada, USA, pp. 637-640, 14-18 August, 2000.

Baker, B., J. Brenguier, and W. Cooper. Unknown Source of Reflectivity from Small Cumulus Clouds. *Cloud Physics Conf.*, Everett, Washington, 1998.

Baker, B.A. Turbulent Entrainment and Mixing in Clouds: A New Observational Approach. *J. Atmos. Sci.*, **104**, no. 4, pp. 387-404, 1992.

Boers, R., H.W.J. Russchenberg, J.S. Erkelens, V.K.C. Venema, A. Van Lammeren, A. Apituley, and S. Jongen. Ground-based remote sensing of stratocumulus properties during CLARA-1996 *J. Appl. Meteorol.*, **39**, no. 2, pp. 169 181, 2000.

Cohn, S.A., R.R. Rogers, S. Jascourt, W.L. Ecklund, D.A. Carter, and J.S. Wilson. Interactions between clear-air reflective layers and rain observed with a boundary layer wind profiler. *Radio Sci.*, **30**, pp. 323-341, 1995.

Davis, A.B., A. Marshak, H. Gerber, and W.J. Wiscombe. Horizontal structure of marine boundary layer clouds from centimeter to kilometer scales. *J. Geophys. Res.,* **104**, pp. 6123-6144, 1999.

Davis, A., A. Marshak, W. Wiscombe, and R. Cahalan. Scale Invariance of Liquid Water Distributions in Marine Stratocumulus. Part I: Spectral Properties and Stationarity Issues. *J. Atmos. Sc.*, **53,** no. 11, pp. 1538-1558, 1996.

Ecklund, W.L., C.R. Williams, P.E. Johnston, and K.S. Gage. A 3-GHz Profiler for Precipitating Cloud Studies. *J. Atmos. Sci.*, **16**, pp. 309-322, 1999.

Erkelens, J.S., S. Jongen, H.W.J. Russchenberg, and M. Herben. Estimation of Cloud Droplet Concentration from Radar, Lidar and Microwave Radiometer Measurements. *Proc. Remote sensing of cloud parameters: retrieval and validation*, Delft, The Netherlands, 21-22 Oct, pp. 107-111, 1999a.

Erkelens, J.S., V.K.C. Venema, H.W.J. Russchenberg, and L.P. Ligthart. Coherent scattering of microwaves by particles, evidence from clouds and smoke. *J. Atmos. Sci*, in press, 1999b.

Fox, N.I., and A.J. Illingworth. The potential of a spaceborne cloud radar for the detection of stratocumulus clouds. *J. Appl. Meteorol.*, **36**, no. 6, pp. 676-687, 1997.

Gage, K.S., C.R. Williams, W.L. Ecklund, and P.E. Johnston. Use of Two Profilers during MCTEX for Unambiguous Identification of Bragg Scattering and Rayleigh Scattering. *J. Atmos. Sci.*, **56**, pp. 3679-3691, 1999.

Frisch, A.S., C.W. Fairall, and J.B. Snider. Measurement of stratus cloud and drizzle parameters in ASTEX with a Ka-band radar and a microwave radiometer. *J. Atmos. Sci.*, **52**, pp. 2788-2799, 1995.

Frisch, U. *Turbulence: the legacy of A.N. Kolmogorov*. Cambridge University Press, 296 p., 1998.

Gossard, E.E., and R.G. Strauch. *Radar Observations of Clear Air and Clouds*. Elsevier, 280 p., 1983.

Gossard, E.E., and R.G. Strauch. The Refractive Index Spectra within Clouds from Forward-Scatter Radar Observations. *J. Atmos. Sci.*, **20**, pp. 170-183, 1981.

Grabowski, W.W., and P. Vaillancourt. Comments on 'Preferential Concentration of Cloud droplets by Turbulence: Effects on the Early Evolution of Cumulus Cloud Droplet Spectra.' *J. Atmos. Sci.*, **56**, pp. 1433-1436, 1999. See also reply on pages 1437-1441.

Van de Hulst, H.C. *Light scattering by small particles*. p. 67 & 70, Dover, New York, 470 p., 1981.

Jameson, A.R., A.B. Konstinski, and R.A. Black. The structure of clouds. *J. Geophys. Res.*, **103**, pp. 6211-6219, 1998.

Lammeren, van, A., et al. Clouds and Radiation: Intensive experimental study of clouds and radiation in the Netherlands (CLARA). *Proc. Remote sensing of cloud parameters: retrieval and validation*, Delft, The Netherlands, 21-22 Oct, pp. 5-10, 1999.

Knight, C.A., and L.J. Miller. Early Radar Echoes from Small, Warm Cumulus: Bragg and Hydrometeor Scattering. *J. Atmos. Sci.*, **55**, no. 18, pp. 2974-2992, 1998.

Korolev, A.V., and I.P. Mazin. Zones of Increased and Decreased Concentration in Stratiform clouds. *J. Appl. Meteorol.*, **32**, pp. 760-773, 1993.

Kozikowska, A, K. Haman, and J. Supronowisz. Preliminary results of an investigation of the spatial distribution of fog droplets by a holographic method. *Quart. J R. Met. Soc.*, **110**, pp. 65-73, 1984.

Malinowski, S.P., M.Y. Leclerck, and D.G. Baumgardner. Fractal Analyses of High-Resolution Cloud Droplet Measurements. *J. Atmos. Sci.*, **51**, no. 3, pp. 397-413, 1994.

Ottersten, H. Radar Backscattering from the Turbulent Clear Atmosphere. *Radio Science*, **4**, no. 12, pp. 1251-1255, 1969.

Paluch, I.R., C.A. Knight, and L.J. Miller. Cloud liquid water and radar reflectivity of non-precipitating cumulus clouds. *J. Atmos. Sci.*, **53**, pp. 1587-1603, 1996.

Pinsky, M.B., A.P. Khain, and Z. Levin. The role of the inertia of cloud drops in the evolution of the spectra during growth by diffusion. *Quarterly J. Royal. Meteorol. Soc.*, **125**, pp. 553-581, 1999.

Politovich, M.K., and W.A. Cooper. Variability of the Supersaturation in Cumulus Clouds. *J. Atmos. Sci.*, **45**, no. 11, pp. 1651-1664, 1988.

Pruppacher, H.R, and J.D. Klett. *Microphysics of Clouds and Precipitation; second edition*. Kluwer, Dordrecht, 954 p., 1997.

Rogers, R.R., and W.O.J. Brown. Radar observations of a major industrial fire. *Bull. Am. Met. Soc.*, **78**, no. 5, pp. 802-814, 1997.

Sassen, K., G.G. Mace, Z. Wang, M.R. Poellot, S.M. Sekelsky, and R.E. McIntosh. Continental Stratus Clouds: A Case Study Using Coordinated Remote Sensing and Aircraft Measurements. *J. Atmos. Sci.*, **56**, pp. 2345-2258, 1999.

Sassen, K., and V. I. Khvorostyanov. Radar probing of cirrus and contrails: Insights from 2D model simulations. *Geophys. Res. Let.*, **25**, no. 7, pp. 975-978, 1998.

Shaw, R.A., W.C. Reade, L.R. Collins, and J. Verlinde. Preferential Concentration of Cloud Droplets by Turbulence: Effects on the Early Evolution of Cumulus Cloud Droplet Spectra. *J. Atmos. Sci.*, **55**, pp. 1965-1976, 1998. See also comment by Grabowski and Vaillancourt (and reply) in *J. Atmos. Sci.*, **56**, pp. 1433-1441, 15 May, 1999.

Squires, K.D., J.K. Eaton. Preferential concentration of particles by turbulence. *Phys. Fluids A,* **3**, no. 5, pp. 1169-1178, 1991.

Tatarski, V.I. *Wave propagation in a turbulent medium*. McGraw-Hill, New York, 285 p., 1961.

Vaillancourt, P.A. *Microscopic approach to cloud droplet growth by condensation*. Ph.D. dissertation, McGill University, Canada, 174 p., 1998.

VanZandt, T.E., J.L. Green, K.S. Gage, and W.L. Clark. Vertical profiles of refractivity turbulent structure function: Comparison of the observations by the Sunset radar with a new model. *Radio Sci.*, **13**, pp. 819-829, 1978.

Venema, V.K.C, H.W.J. Russchenberg, A. Apituley, A. van Lammeren, and L.P. Ligthart. Cloud boundary height measurements using lidar and radar. *Physics and Chemistry of the Earth.*, **24**, no. 2, pp. 129-134, 2000.

Wit, de J.J.M., R.J.P. Baedi, J.S. Erkelens, H.W.J. Russchenberg, and J.P.V. Poiares Baptista. Development of retrieval algorithms of cloud parameters from radar and lidar based on the CLARE data set. *Proc. Remote sensing of cloud parameters: retrieval and validation*, Delft, The Netherlands, 21-22 Oct, pp. 83-88, 1999.